Classification of emerging patterns in self-assembled two-dimensional magnetic lattices

Ehsan Norouzi, Audrey A. Watkins ©, and Osama R. Bilal ©[*]

Wave Engineering through eXtreme & Intelligent matTEr Laboratory, Department of Mechanical Engineering,
University of Connecticut, Storrs, Connecticut 06269, USA

Self-assembled granular materials can be utilized in many applications such as shock absorption and energy harvesting. Such materials are inherently discrete with an easy path to tunability through external applied forces such as stress or by adding more elements to the system. However, the self-assembly process is statistical in nature with no guarantee for repeatability, stability, or order of emergent final assemblies. Here we study both numerically and experimentally the two-dimensional self-assembly of free-floating disks with repulsive magnetic potentials confined to a boundary with embedded permanent magnets. Six different types of disks and seven boundary shapes are considered. An agent-based model is developed to predict the self-assembled patterns for any given disk type, boundary, and number of disks. The validity of the model is experimentally verified. While the model converges to a physical solution, these solutions are not always unique and depend on the initial position of the disks. The emerging patterns are classified into monostable patterns (i.e., stable patterns that emerge regardless of the initial conditions) and multistable patterns. We also characterize the emergent order and crystallinity of the emerging patterns. The developed model along with the self-assembly nature of the system can be key in creating re-programmable materials with exceptional nonlinear properties.

I. INTRODUCTION

Granular media have inspired an extensive number of studies on the interplay between nonlinearity and discreteness [1] with many potential applications in shock absorption, acoustic sensing, switching, and energy harvesting [1–6]. In addition to their potential as a fascinating platform to study nonlinear dynamics [7–10], they can be easily prototyped from simple basic particles such as beads and disks. The inherent discreteness in such media makes them an ideal candidate for fabrication through self-assembly processes [10–17,17–21]. However, the statistical nature of the self-assembly process can hinder their practicality as the final assembly depends highly on the initial positions of the system elements [22,23]. Even for highly repeatable patterns, a certain amount of disorder usually emerges within the assembly. The present study considers the interplay between the symmetry of granular elements, their confining boundary shape, and resulting final pattern. The repeatability, stability, and inherent order in the self-assembled emergent patterns are studied.

In this paper we study the self-assembly of various types of free-floating magnetic disks in two dimensions confined to a fixed boundary with embedded magnets. In particular, the repeatability, stability, and crystallinity of these emerging patterns under different boundary conditions is considered. The free-floating disks are subject mainly to repulsive magnetic interactions among themselves and their confining boundary in two dimensions (i.e., with negligible friction). We develop a numerical model to predict the final assembly of the free-floating disks based on an agent-based model. We consider six different types of disks, with the number of embedded permanent magnets ranging from 1 to 6. We consider seven types of boundaries, with the number of sides varying from 3 (triangle) to 8 (octagon) in addition to a circular boundary (Fig. 1). The model is executed multiple times with different initial positions of the disks and their final assembly after convergence is recorded. The final assemblies are classified as monostable (the same pattern emerges regardless of the initial position of the disks) or multistable (where the initialization plays a crucial rule in the final pattern) patterns. To classify the stability of these emerging patterns as monostable or multistable, we calculate the relative position between the disks (i.e., relative distance and angles between the disks) at their
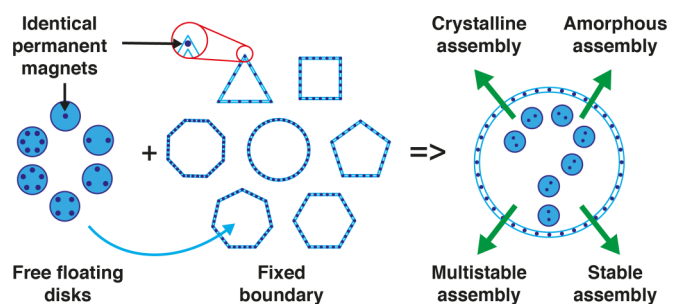

FIG. 1. Concept. The self-assembly of six disk types (left) with embedded identical magnets is considered. The disks are confined to different boundary shapes (middle). The boundaries also have identical permanent magnets with the same polarity as the disks. The final self-assembly can be mono- or multistable, crystalline or amorphous depending on the number and type of disks and the boundary shape.

_____
[*]osama.bilal@uconn.edu

final assemblies. We consider a pattern to be monostable if the same pattern emerges for the same number of disks and boundary type, despite the different random initial positions of the disks; otherwise, the pattern is considered multistable. In addition, if a pattern is monostable, we quantify the variability in the final positions of the disks between various simulations with different initial positions.

II. AGENT-BASED MODEL

An agent-based model [24] is developed to numerically simulate the self-assembly of free-floating disks confined within different boundaries with magnetic potentials in two dimensions. Each disk acts as an *autonomous agent* that has the ability to make a decision about its position and orientation, on its own. The disks individually assess their utility function and make the decision based on predefined rules. The utility function E_{disk_i} that each disk tries to minimize represents the absolute value of the repulsive forces they experience from all the other agents, in addition to the boundary magnets. The decisions available to each agent include a move of a distance ϵ from its current position to the left, right, up, or down or a valid combination of two directions (i.e., up and left or down and right). The agent calculates the change in the utility function based on the possible moves and executes a jump to the new position with the lowest possible energy. Disks are penalized with a high utility function cost not to consider a jump outside the predefined boundary. This rule guarantees the confinement of all disks to the boundary and simulates the presence of a physical boundary. In the case of having more than one magnet per disk (i.e., dimer, trimers, etc.) the disk also evaluates a change in its orientation angle, while staying in the same position, and chooses the orientation with the lowest energy. The disks start at random positions and the model evolves autonomously based on the interactions between the different agents according to the predefined rules. The simulation terminates once the change in the total energy of the system E_{tot} is negligible.

The total energy of the system is calculated as the summation of the energy of individual disks, which takes into account the repulsive forces between the permanent magnets following an inverse power law. All magnets are oriented in the same way (e.g., north pole facing up); therefore, all magnets act as monopoles in two dimensions. The total energy of the system can be represented as

$$E_{tot} = \sum_{i=1}^{N} \{E_{disk_i}\}, \quad (1)$$

where the individual disk utility function E_{disk_i} is

$$E_{disk_i} = \sum_{w=1}^{M} \left\{ \sum_{j=1, j \neq i}^{N} |A d_{w_i j}^{\gamma}| + \sum_{k=1}^{B} |A d_{w_i k}^{\gamma}| \right\}, \quad (2)$$

where N is the number of free-floating disks (i.e., agents), $M \in [1, 2, \ldots, 6]$ is the number of magnets per disk, $d_{w_i j}$ is the distance between the position of magnet i in disk w and magnet j, B is the number of boundary magnets, and $A = 3\mu\beta^2/4\pi$, where μ is the permeability of air and β is the magnetic moment [6].

III. MODEL VALIDATION

We simulate the self-assembly of free-floating disks for the combination of the following cases: (i) seven different boundaries with the number of sides ranging from 3 (triangle) to 8 (octagon) in addition to a circular boundary and (ii) six different disk configurations (one magnet, two magnets, three magnets, four magnets, five magnets, and six magnets) per disk. In each of these 42 configurations (seven boundaries and six disk types), we simulate the self-assembly of disks from 1 to 50 disks per assembly, totaling 2100 different simulations. Each of these 2100 simulations is repeated for ten different random initial disks' positions. We record the final position in each of the 21 000 simulations and analyze the emerging patterns using different indices. The boundary side length S_x, where x represents the number of sides is $S_3 = 176$ mm, $S_4 = 200$ mm, $S_5 = 176$ mm, $S_6 = 150$ mm, $S_7 = 130$ mm, and $S_8 = 114$ mm and the circle radius $R = 150$ mm. The number of magnets per side on all the boundaries is equal to 6, except for the square boundary (7). The number of magnets on the circle is 38. The magnet parameters are $A = 6.6 \times 10^{-11}$ and $\gamma = -4$.

The convergence of the agent-based model is analyzed by considering the average energy per disk defined as $\bar{E}_{tot}^*/N$, where $\bar{E}_{tot}$ is the total energy of the system excluding the boundary energy [i.e., the second term in Eq. (2)]. The ( )* indicates the lowest energy values between the ten simulations of each identical case (i.e., with random initial positions of the same number of disks, disk type, and boundary shape). Figure 2 shows the $\bar{E}_{tot}^*/N$ separated by boundary type. The lower corner of Figs. 2(a) and 2(c)–(h) shows the corresponding boundary shape. For all boundaries, we observe a constant rise in the average energy per disk as the number of disks is increased across all disk types (1–6 magnets per disk). The rise in the energy per disk is consistent with the increase of disk density calculated as the number of disks in a constant area enclosed by the boundary. The only discrepancy emerges in the average energy per disk for the triangular boundary in the vicinity of the self-assembly of 15 disks. This dip in the average energy per disk is consistent for all disk types, suggesting a boundary anomaly rather than a modeling one. By closely examining the emerging patterns for the number of disks between 10 and 20, the extreme dependence of the final pattern on the initial disk positions is noted. The three acute angles at the corners of the triangle along with the fixed magnets in their vicinity create an energy barrier that can only be penetrated in special cases (when the total repulsion force acting on the disk closest to the triangle corner is greater than the repulsion force of the three corner magnets). Once a disk crosses this energy barrier, it cannot exit, as its total energy is smaller at the corner. This can be observed by closely considering the emerging patterns with the lowest total energy when simulating the self-assembly of 14–16 disks with two magnets per disk. The emerging patterns in the case of 14 and 15 disks are identical, with the exception of the vacant vs occupied corner [Fig. 2(b)]. The added disk at the corner (in the case of 15 disks assembly) does not add any significant energy to the total energy of the system when normalized by the number of disks. By adding an extra disk (i.e., 16 disks) the pattern changes, in comparison to the case with 15 disks,
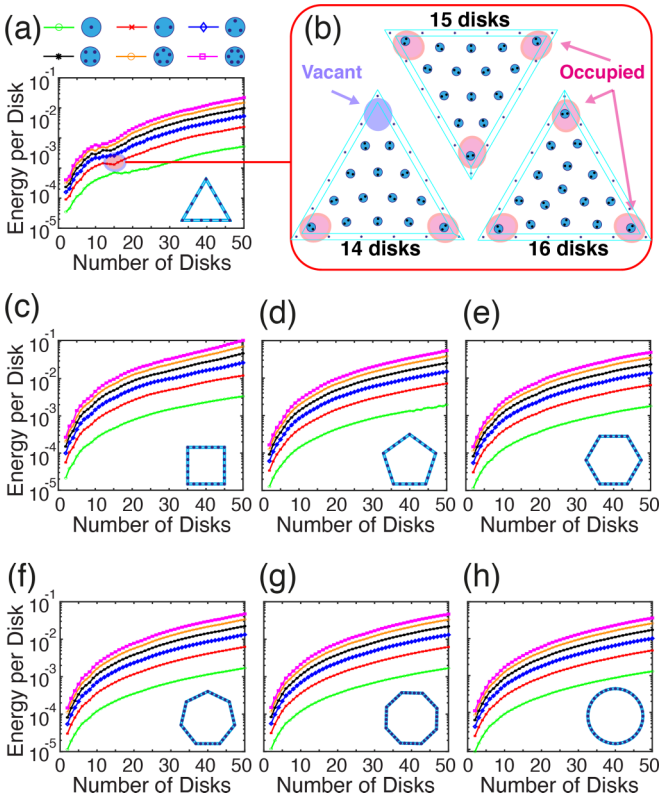
FIG. 2. Model convergence. The lowest average energy $\bar{E}_{tot}^{*}/N$ in ten different self-assembly numerical simulations for each boundary, type of disk, and number of disks (total 21K) for (a) triangular, (c) square, (d) pentagonal, (e) hexagonal, (f) heptagonal, (g) octagonal, and (h) circular boundaries. (b) shows the reason for the dip in the energy levels for 14–16 disks with dimers starting to fully occupy the corners of the triangular boundary.

IV. EXPERIMENTAL VERIFICATION

While the numerical validation through the average energy per disk suggests a consistent convergence of the model in all cases, it motivates the following question: While the model converges, does it simulate reality? In other words, *is the solution physical?* To experimentally verify the numerically simulated self-assembly and its final patterns, seven studied boundaries are fabricated with the same parameters as the simulations out of acrylic glass using a laser cutter (Full-spectrum 24 pro-series). The magnets embedded within the boundary and the magnets in the disks are oriented with the north pole facing upward. To minimize friction, a glass slide is attached at the bottom of each disk and floated on an air bearing (New way S1030002). The disks experience minimal to no friction as they hover over a thin layer of laminar flow once the air bearing is activated (similar to an air hockey table). The motion of the disks and the resulting images are captured using a computer vision camera (Blackfly S USB3) and are analyzed using the digital image correlation software (DICe).
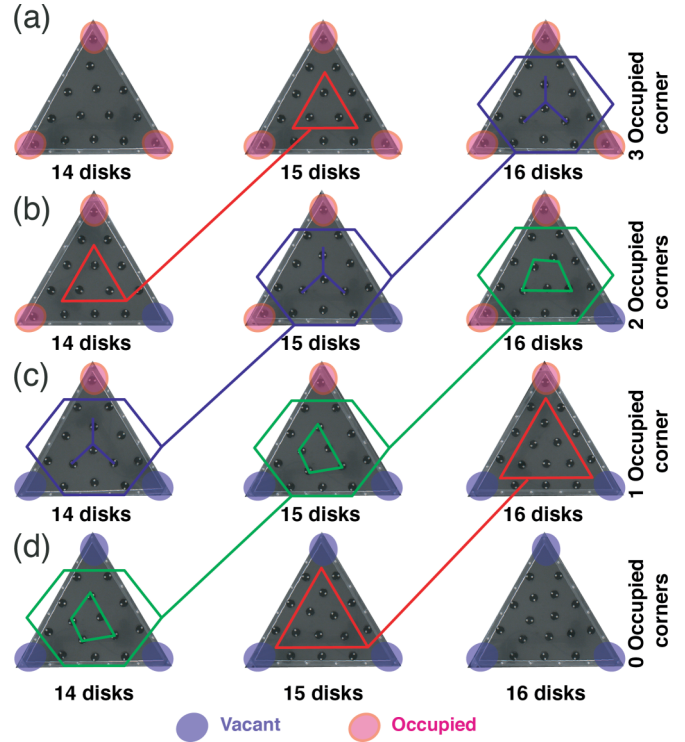

FIG. 3. Experimental verification. Experimentally assembled 14–16 dimers (disks with two magnets each) with (a) all the corners of the triangular boundary occupied and (b) two, (c) one, and (d) zero corners occupied. The same emerging pattern is highlighted with various shapes. For example, 16 disks with 3 occupied triangle corners is the same pattern with 15 disks and 2 occupied triangle corners and 14 disks with 1 corner occupied, all of which resemble a peace sign with three magnets parallel to the triangle sides.

We start the experimental verification by considering the self-assembly of 14–16 disks with two magnets each within the triangular boundary [the same case proved to be challenging in the numerical simulation in Figs. 2(a) and 2(b)]. We first position the triangular boundary on the air bearing surrounding the disks at random positions relative to each other and to the boundary. The air bearing is then activated to allow the disks to free-float, significantly reducing the friction between the disks and the bearing surface and allowing the repulsion forces between the magnets to dominate the repositioning process. The system is left unperturbed for 15 s (i.e., enough time for the disks to reach their equilibrium positions) and the resulting pattern is recorded. Afterward, the system is significantly perturbed, forcing every disk to leave its position and to form a new equilibrium state. The process is repeated for 100 times taking an image each time the system reaches the equilibrium point. The same phenomenon, previously indicated in the numerical verification section, is observed. The final assembly depends greatly on the initialization position. The disks can, and do, enter the corner energy potential well and can easily stay inside. In all three cases (i.e., 14–16 disks), the four different potential patterns ranging from all corners (occupied to vacant) are stable and physical and do take place (Fig. 3). Remarkably, the same pattern emerges in the different disk numbers if we omit the corner confined disks. For
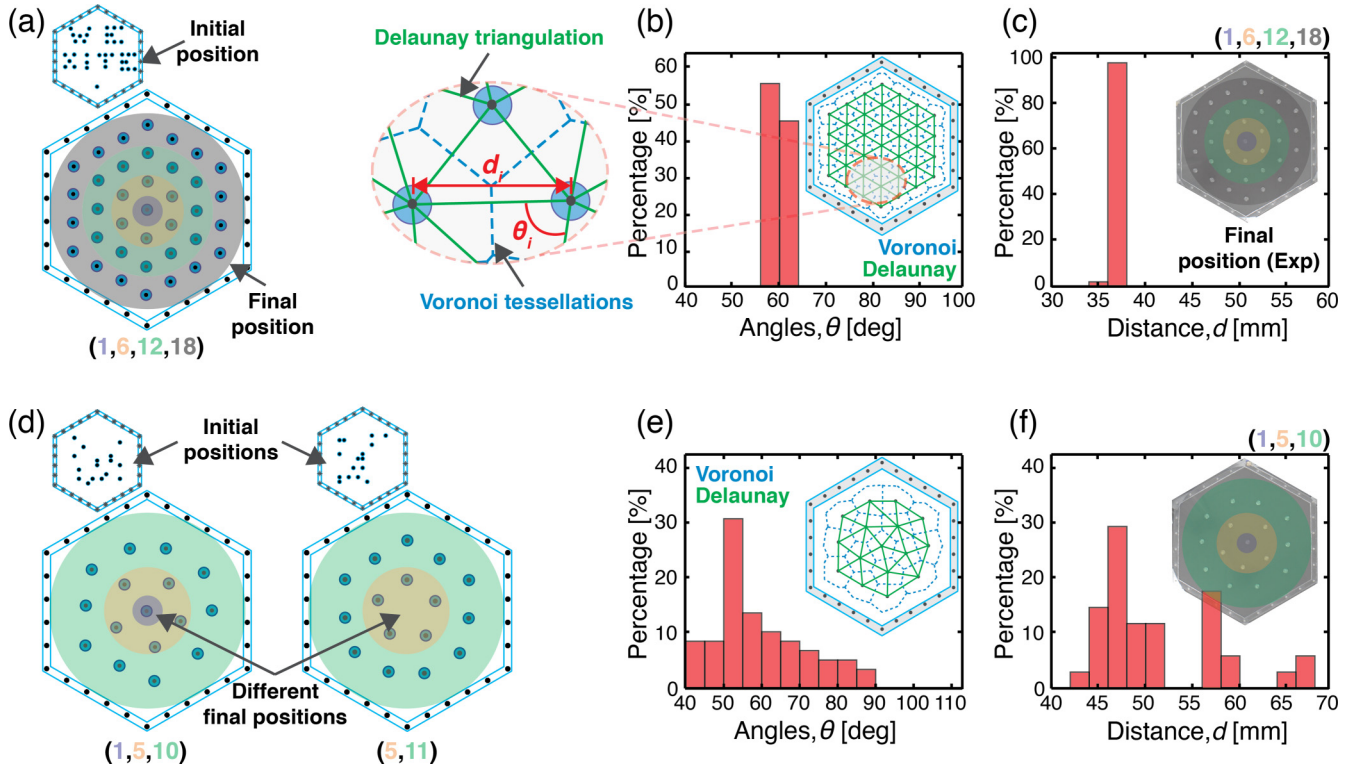
and the amount of energy per disk starts to rise systematically again.

FIG. 4. Analysis of the emerging pattern. (a) Initial position of 37 disks within a hexagonal boundary writing "We-Xite" and their numerically calculated final assembly as a triangular lattice. An overlay of four concentric circles are used to count the number of disks within the layers of the final assembly to distinguish different emerging patterns. (b) Histogram of the angles between the disks in their final assembly position using the Delaunay triangulation. The inset shows the final assembled pattern with superimposed Delaunay triangulation and Voronoi tessellation. (c) Histogram of the distances between 37 disks in their final assembly position using the Delaunay triangulation. The inset shows an overlay of the same four concentric circles to count the layers within the experimentally assembled pattern. (d) Two initial positions of 16 disks within the same hexagonal boundary and their numerically calculated final assembly into two different patterns. An overlay of three (left) and two (right) concentric circles are used to count the number of disks within the layers of the final assembly to distinguish different emerging patterns. (e) Histogram of the angles between the disks in their final assembly position using the Delaunay triangulation. (f) Histogram of the distances between 16 disks in their final assembly position using the Delaunay triangulation. The inset shows an overlay of the same three concentric circles to count the layers within one of the experimentally assembled patterns.

example, the pattern of 16 disks with three occupied corners [Fig. 3(a), right] is identical to the pattern of 15 disks with two occupied corners [Fig. 3(b), middle] and the 14 disks with one occupied corner [Fig. 3(c), left]. It is worth noting however, if we omit the corners of the triangle, we turn it into a six-sided polygon, defeating the purpose of the study.

V. ANALYSIS OF THE EMERGING PATTERNS

With the model convergence into plausible assemblies experimentally verified, we start analyzing the emerging patterns, in particular, comparing the emerging patterns of the same number of disks to determine the pattern repeatability, stability, and inherent order with different initial positions. We attempt to classify the emerging patterns into two categories: (i) monostable, where, regardless of the initial position of the disk, the exact pattern always emerges (with minute variation), and (ii) multistable, where, depending on the initial positions, the solution can bifurcate into two or more stable assemblies. To perform our analysis we depend on two metrics: (a) the number of disks within concentric layers from the center of the pattern to determine if the patterns are similar

or different and (b) the distances and angles between disks in similar patterns to estimate any long-range order within the pattern (i.e., crystallinity).

VI. PATTERN STABILITY

To present these two metrics, we consider the self-assembly of 16 and 37 disks within a hexagonal boundary. Each disk has one embedded permanent magnet (Fig. 4). We start by randomly positioning the disks within the boundary. In the case of the 37 disks, regardless of the initial position, the emerging pattern is always a triangular packing of the disks. Even when the initial position of the disks reads the laboratory name, "We-Xite" [Fig. 4(a)], it emerges into a perfect triangular lattice (see movie 1 in [25]). In the case of the 16 disks, two random initial positions are shown [Fig. 4(d)] emerging into two topologically distinctive patterns. The left pattern in Fig. 4(d) has a disk at its center, while the pattern on the right does not. To distinguish between two such patterns, we use concentric rings starting from the boundary center to count the number of layers within the pattern and the number of disks within each layer. For example, the pattern in Fig. 4(d) (left)
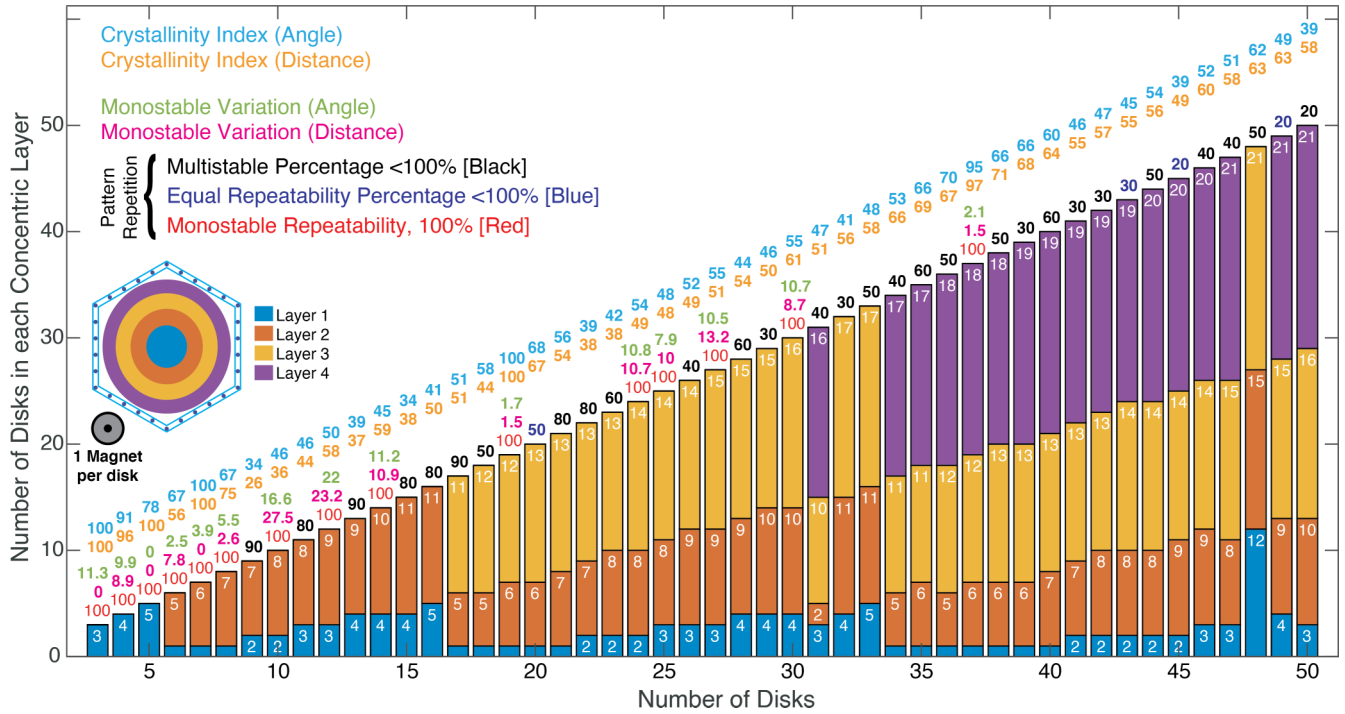
FIG. 5. Pattern classification. The bars are the number of disks within the concentric layers in a hexagonal boundary for disks with one magnet per disk. The layer order is presented in the inset. The numbers on top of the bars are the repeatability percentage of the pattern. The monostable patterns with 100% repeatability are written in red. For monostable patterns, the variation in the distance between the disk positions (magenta) and angles (green) are presented right above their 100%. The top two rows represent the crystallinity index for the distance (orange) and angle (light blue) between the disks in the reported pattern. The layer counting parameters are $\epsilon = 17$ mm and $\delta = 14$ mm.

can be decoded into (1,5,10), meaning in the left pattern there exist one disk in the center layer, five disks in the middle layer, and ten disks in the outermost layer. Similarly, the pattern on the right would be (5,11): only two layers, with 5 at the center and 11 in the outer layer. The emerging patterns in both cases (37 and 16 disks) are experimentally verified [Figs. 4(c) and 4(f) (inset)]. The experimental images are analyzed in the same way showing identical numbers of layers and occupying disks within each layer. The layers within the emerging patterns are estimated as follows. (i) Locate the disk closest to the center of the boundary. (ii) The first layer covers that disk plus a distance ϵ. (iii) Count the number of disks within that circle as layer one and then remove these disks and start over; until all disks are counted. If two layers are closer than a distance δ we merge the two layers into one. We apply the layer counting principle on the emerging patterns in each of the 21 000 cases (seven boundaries, six disk types, 1–50 disks, ten times each). If the emerging patterns have the same layer count and the same number of disks in each layer, despite the different initial positions of the disks, the pattern is considered monostable; if not, it is multistable.

VII. PATTERN ORDER

In addition to the repeatability of the assembly, we quantify the crystallinity of the emerging patterns. We calculate the distance between disks d and the angles θ between them using Delaunay triangulation. We represent these angles and distances in a histogram for both the 37 [Figs. 4(b) and 4(c)] and the 16 [Figs. 4(e) and 4(f)] disks cases. Due to the clear

long-range order in the case of 37 disks with the triangular lattice, the distances between all the disks are almost identical (between 36 and 38 mm) and the angles between the disks are almost all identical (between 55° and 65°). In contrast, in the case of 16 disks, both angles and distances span a much larger range of values (between 35 and 68 mm and between 40° and 90°). We define our metric of crystallinity as the summation of the two highest histogram bars. In the case of 37 disks, the crystallinity index is approximately equal to 100% for the 37 disks case in both angle and distance distributions (97% for distance and 95% for angles). In contrast, the crystallinity index for the 16-disk case is 50% for distance and 41% for angles. Such an index can be used to easily identify patterns with high crystallinity for further investigations, particularly when combined with a high repeatability percentage.

VIII. NUMERICAL CLASSIFICATION PLOTS

To classify the emerging patterns accordingly, we plot the calculated metrics of repeatability or stability of the assembly and the crystallinity indices for both angle and distance in one plot per boundary per disk type. An example plot of our classification plots for a hexagonal boundary and one magnet per disk is presented in Fig. 5. The bar colors represent the different layers starting from the center of the pattern. The bar height, and the number within, represents the number of disks in that particular layer. Immediately on top of the bars for each pattern is its repeatability (the percentage of times where the pattern with the same number of layers and disks within each layer emerges). The multistable pattern percentages are
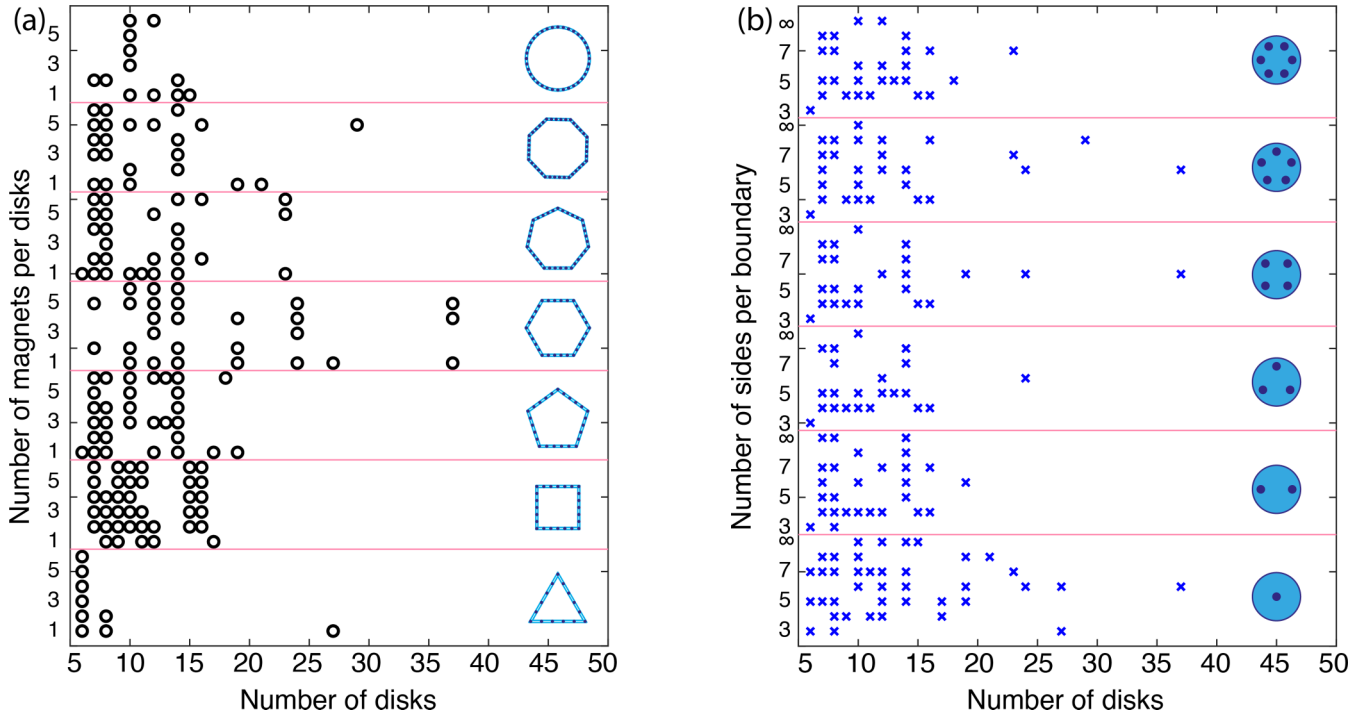
FIG. 6. Monostable patterns. All the patterns proven stable in both numerical simulation and experimental testing are grouped by (a) boundary shape and (b) disk type. The y axis in (a) represents the number of magnets within each disk starting with one magnet per disk until six magnets per disk. The y axis in (b) represents the number of sides per boundary starting with the triangular boundary (three sides) to the octagonal boundary (eight sides) and the circular boundary (infinite sides). The markers in both panels indicate a stable pattern for a given boundary shape, disk type, and number of disks.

black. If more than one pattern occurs, we present the pattern with the higher repeatability. If two patterns have the same repeatability percentage the percentage is written in dark blue. In the case of a monostable pattern, the 100% repeatability is written in red. Additionally, for the numerically monostable patterns, we calculate the variation in the distance and angles between the final positions of the disks in the multiple runs; both numbers are located above the 100% repeatability rate of the monostable patterns. The crystallinity indices for all patterns (mono- or multistable) are located at the very top of the layering bars. Figure 5 is only one example of 42 plots (six disk types in seven boundaries). The remaining 41 classification plots are included in the Supplemental Material [25]. In the case of more than one magnet per disk, a variation in the phase angle of the disk is also included at the top of the plot for each case. It is worth noting that both centered hexagonal numbers [or magic numbers following the equation of $3n(n-1)+1$, where n is the number of disks per side [26]] of 19 and 37 appear as monostable patterns within a hexagonal boundary (100% repeatability), with very high crystallinity indices greater than 95% (Fig. 5), indicating the presence of a highly *ordered* lattice. For the number of disks 24 and 27, for example, the repeatability index is 100%; however, the crystallinity indices are rather low, less than 55%, indicating a monostable *amorphous* assembly. It is also worth noting that in the case of disks with more than one magnet, the orientation angle of the disk plays a significant role in its energy minimization. Such orientation dependence can give rise to intriguing physics within the system such as frustration [21,27].

IX. EXPERIMENTALLY VERIFIED STABILITY

Finally, the stability or repeatability of the emerging patterns is tested experimentally. The disks are placed within the boundary, with the embedded magnets, at random positions. The air bearing is then activated to allow the disks to free-float, significantly reducing the friction between the disks and the bearing surface and allowing the repulsion forces between the magnets to dominate the repositioning process. The system is left unperturbed for 15 s (i.e., enough time for the disks to reach their equilibrium positions) and the resulting pattern is recorded. Afterward, the system is perturbed significantly, forcing every disk to leave its position and to form a new equilibrium state. The process is repeated ten times, taking an image each time the system reaches the equilibrium point. The ten images are then compared with each other to determine the repeatability of the pattern. The same layer counting principle applied in the numerical simulations is followed for the resulting images. Many of the patterns that were predicted by our numerical analysis proved stable. However, a similar amount turned out to be multistable. The patterns proven stable in experiments along with the numerical analysis are included in Fig. 6. Remarkably, a very small number of patterns are proven repeatable within the triangular boundary. This can be justified by the corner observation discussed in Fig. 3. In addition, the emerging patterns within the circular boundary proved not very repeatable. Mainly, as observed in the experiments, it is very easy for a disk to migrate from one layer to another, deeming the pattern multistable.

X. CONCLUSION

The two-dimensional self-assembly of free-floating disks with different numbers of embedded magnets confined to different fixed boundaries with constant magnetic potentials was studied. An agent-based model has been developed to simulate the self-assembly process, where each disk is represented as an agent trying to minimize its *own* energy. This individualistic behavior of each disk reduces the total energy of the system to a stable and physical final pattern. The validity of the model was verified experimentally using an air-bearing table to minimize friction and clearly elucidate the repulsive magnetic interaction between the disks. While the model converges to a physical solution, these solutions are not unique and depend on the initial position of the disks. Such dependence is classified into stable patterns that emerge regardless of the initial conditions (monostable patterns and multistable patterns). The crystallinity of the emerging patterns was also characterized. The developed model along with the self-assembly nature of the system can be key in creating reprogrammable materials with exceptional properties [11]. In addition, the inherent nonlinear potentials between the differ- ent disk types can be harnessed to demonstrate phenomena with no linear parallel such as amplitude-dependent energy management.

The data that support the findings of this study are available within the article and the Supplemental Material [25]. Additional data are available from the corresponding author upon reasonable request.

[1] M. A. Porter, P. G. Kevrekidis, and C. Daraio, Granular crystals: Nonlinear dynamics meets materials engineering, Phys. Today **68** (11), 44 (2015).

[2] A. Mehrem, N. Jiménez, L. J. Salmerón-Contreras, X. García-Andrés, L. M. García-Raffi, R. Picó, and V. J. Sánchez-Morcillo, Nonlinear dispersive waves in repulsive lattices, Phys. Rev. E **96**, 012208 (2017).

[3] O. V. Gendelman and A. F. Vakakis, Introduction to a topical issue 'nonlinear energy transfer in dynamical and acoustical systems', Philos. Trans. R. Soc. A **376**, 20170129 (2018).

[4] E. Kim and J. Yang, Wave propagation in granular metamaterials, Funct. Composites Struct. **1**, 012002 (2019).

[5] V. Ramakrishnan and M. J. Frazier, Transition waves in multistable metamaterials with space-time modulated potentials, Appl. Phys. Lett. **117**, 151901 (2020).

[6] A. A. Watkins and O. R. Bilal, Demultiplexing infrasound phonons with tunable magnetic lattices, Front. Mater. **7**, 606877 (2020).

[7] C. Chong, Y. Wang, D. Maréchal, E. G. Charalampidis, M. Molerón, A. J. Martínez, M. A. Porter, P. Kevrekidis, and C. Daraio, Nonlinear localized modes in two-dimensional hexagonally-packed magnetic lattices, New J. Phys. **23**, 043008 (2021).

[8] M. Molerón, C. Chong, A. J. Martínez, M. A. Porter, P. G. Kevrekidis, and C. Daraio, Nonlinear excitations in magnetic lattices with long-range interactions, New J. Phys. **21**, 063032 (2019).

[9] S. Shankar, A. Souslov, M. J. Bowick, M. C. Marchetti, and V. Vitelli, Topological active matter, arXiv:2010.00364.

[10] B. C. van Zuiden, J. Paulose, W. T. Irvine, D. Bartolo, and V. Vitelli, Spatiotemporal order and emergent edge currents in active spinner materials, Proc. Natl. Acad. Sci. USA **113**, 12919 (2016).

[11] U. Culha, Z. S. Davidson, M. Mastrangeli, and M. Sitti, Statistical reprogramming of macroscopic self-assembly with dynamic boundaries, Proc. Natl. Acad. Sci. USA **117**, 11306 (2020).

[12] W. Wang, J. Giltinan, S. Zakharchenko, and M. Sitti, Dynamic and programmable self-assembly of micro-rafts at the air-water interface, Sci. Adv. **3**, e1602522 (2017).

[13] C. Reichhardt and C. O. Reichhardt, Reversibility, pattern formation, and edge transport in active chiral and passive disk mixtures, J. Chem. Phys. **150**, 064905 (2019).

[14] M. X. Lim, A. Souslov, V. Vitelli, and H. M. Jaeger, Cluster formation by acoustic forces and active fluctuations in levitated granular matter, Nat. Phys. **15**, 460 (2019).

[15] J. Hernández-Rojas, D. Chakrabarti, and D. Wales, Self-assembly of colloidal magnetic particles: Energy landscapes and structural transitions, Phys. Chem. Chem. Phys. **18**, 26579 (2016).

[16] R. Messina and I. Stanković, Self-assembly of magnetic spheres in two dimensions: The relevance of onion-like structures, Europhys. Lett. **110**, 46003 (2015).

[17] R. Messina, S. Aljawhari, L. Bécu, J. Schockmel, G. Lumay, and N. Vandewalle, Quantitatively mimicking wet colloidal suspensions with dry granular media, Sci. Rep. **5**, 10348 (2015).

[18] J. Schockmel, E. Mersch, N. Vandewalle, and G. Lumay, Melting of a confined monolayer of magnetized beads, Phys. Rev. E **87**, 062201 (2013).

[19] S. Merminod, M. Berhanu, and E. Falcon, Transition from a dissipative to a quasi-elastic system of particles with tunable repulsive interactions, Europhys. Lett. **106**, 44005 (2014).

[20] F. Martínez-Pedrero, Static and dynamic behavior of magnetic particles at fluid interfaces, Adv. Colloid Interface Sci. **284**, 102233 (2020).

[21] E. Opsomer, S. Merminod, J. Schockmel, N. Vandewalle, M. Berhanu, and E. Falcon, Patterns in magnetic granular media at the crossover from two to three dimensions, Phys. Rev. E **102**, 042907 (2020).

[22] B. A. Grzybowski, H. A. Stone, and G. M. Whitesides, Dynamic self-assembly of magnetized, millimetre-sized objects rotating at a liquid–air interface, Nature (London) **405**, 1033 (2000).

[23] G. M. Whitesides and B. Grzybowski, Self-assembly at all scales, Science **295**, 2418 (2002).

[24] E. Bonabeau, Agent-based modeling: Methods and techniques for simulating human systems, Proc. Natl. Acad. Sci. USA **99**, 7280 (2002).

[25] See Supplemental Material at http://link.aps.org/supplemental/10.1103/PhysRevE.104.044902 for detailed assembly maps for different disk symmetries within the considered boundaries and for a movie showing emergence of a triangular lattice.

[26] M. Gardner, Mathematical games, Scientific American **231**, 116 (1974).

[27] A. A. Watkins, A. Eichelberg, and O. R. Bilal. Exploiting localized transition waves to tune sound propagation in soft materials, arXiv:2109.10178 (2021).